Size-dependent excitation spectra and energy transfer in Tb3+-doped Y2O3 nanocrystalline

Qingyu Meng, Baojiu Chen, Wu Xu, Yanmin Yang, Xiaoxia Zhao et al.

Citation: J. Appl. Phys. **102**, 093505 (2007); doi: 10.1063/1.2803502
View online: http://dx.doi.org/10.1063/1.2803502
View Table of Contents: http://jap.aip.org/resource/1/JAPIAU/v102/i9
Published by the American Institute of Physics.

Size-dependent excitation spectra and energy transfer in Tb^{3+}-doped Y_2O_3 nanocrystalline

Qingyu Meng, Baojiu Chen,[a] Wu Xu, Yanmin Yang, Xiaoxia Zhao, Weihua Di, Shaozhe Lu, and Xiaojun Wang
Lab of Excited State Processes, Changchun Institute of Optics, Fine Mechanics and Physics, Chinese Academy of Sciences, Changchun 130033, People's Republic of China and Graduate School of the Chinese Academy of Sciences, Beijing 100039, People's Republic of China

Jiashi Sun, Lihong Cheng, Tao Yu, and Yong Peng
Department of Physics, Dalian Maritime University, Dalian, 116026, People's Republic of China

(Received 7 March 2007; accepted 10 September 2007; published online 2 November 2007)

Nanocrystal Y_2O_3 powders with different grain sizes and various doping concentrations of Tb^{3+} were prepared by an autocombustion reaction. The size and surface effects on the $4f$-$5d$ transitions and energy transfers between Tb^{3+} ions were studied by using x-ray diffraction, transmission electron microscopy, fluorescent spectra, and luminescent decay. It was found that the excitation spectra are composed of two parts: one is the contribution from the Tb^{3+} at/near the nanoparticle surfaces; another is from the Tb^{3+} inside the nanoparticles. The study on the concentration quenching and luminescent decay indicated that the energy transfers depopulating the $^5D_3$ and $^5D_4$ level were assigned to the mechanisms of electric dipole-dipole and exchange interaction, respectively. The size confinement greatly affects the energy transfer quenching the emission from the $^5D_3$ level, but slightly affects the energy transfer quenching the emission from the $^5D_4$ level.
 [DOI: 10.1063/1.2803502]

I. INTRODUCTION

Rare earth (RE)-doped inorganic luminous materials have been extensively used in display, lighting, optocommunication, laser device, x-ray sensor, and so on.[1–7] The performance of these materials has been increasingly improved and many efforts have been devoted to them. It was discovered that nanosized materials have special properties different from the bulk ones, and so have attracted much attention for study, but some basic physical understandings of the surface states and quantum confinements in the RE-doped nanomaterials are still unclear. Moreover, up to now, very few of the practical applications of RE doped nanomaterials have been reported. Therefore, exploring the basic theories and applications of nanosized materials has become an interesting topic. With the development of the display technique, a demand for a display screen with high resolution is also increasing. Undoubtedly, the nanophosphors would be helpful for improving the display resolution, packing density, and luminescent uniformity of phosphors on the screens. In addition, nanosized luminescent particles could also be used in the integrated optics field to realize optical switches and some optical logical functional cells.[8,9] It has been expected that nanostructure could cause a quantum confinement to the RE ions inside the nanoparticles, but the quantum confinement can hardly be observed owing to the small Bohr radius of $4f$-electrons of RE ions. A widely known fact, the RE-doped nanosized materials usually show a lower fluorescent yield due to numerous surface defects which can quench the luminescence.[10] Though the RE-doped nanosized materials with high quantum efficiency are difficult to obtain, it is not to say that RE-doped nanosized materials are hopeless. Surely a theoretical margin of quantum efficiency, which is close to the quantum efficiency of corresponding bulk, could be achieved via effective surface passivation.[11] On the other hand, comprehensive understanding of the surface state and quantum confinement of nanoparticles would be beneficial to the design and processing of nanosized materials.

The aim of this work is to investigate the spectral difference between Tb^{3+} ions located at/near the surface and inside the nanoparticles, and how the size confinement influences the energy transfer between Tb^{3+} ions. For these purposes, nanocrystal Y_2O_3 powders with different grain sizes and various doping concentrations of Tb^{3+} were prepared using a solution combustion synthesis procedure. The large-sized samples were obtained by calcining the corresponding nanoparticle samples at a high temperature. The crystal structure, morphology, and luminescence were studied by means of x-ray diffraction (XRD), transmission electron microscopy (TEM), fluorescent spectra, and fluorescent dynamics. It was found that the excitation bands corresponding to the $4f$-$5d$ transitions of Tb^{3+} ions change with the average particle size. The types of energy transfers between Tb^{3+} ions were identified by numerical fittings based on the concentration quenching curves. The experimental results indicated that particle size slightly affects the energy transfer between $^5D_4$ levels. However, the energy transfer originating from the $^5D_3$ level is strongly dependent on the particle size. The effect of particle size on the energy transfer was assigned to the size confinement of nanoparticles.

[a]Author to whom correspondence should be addressed. Telephone/FAX: +86-411-84728909. Electronic mail: chenmbj@sohu.com

II. EXPERIMENT

The nanocrystal Y_2O_3:Tb powders studied were prepared by a chemical autocombustion reaction. In the preparation, analytical grade $Y(NO_3)_3$, $Tb(NO_3)_3$, and glycine were dissolved in distilled water and mixed together to form the precursor solution. The precursor solution was heated in an electronic furnace to evaporate the water. The autocombustion reaction occurred when the water was evaporated off. After scorching combustion, the white leftover powders were collected for further processing. The nanoparticle size could be controlled by adjusting the molar ratios of NO_3^- to glycine. A detailed preparation process is given elsewhere.[12–14] In this study, the doping concentration of Tb^{3+} is described by $\{[Y]:[Tb]=(1-X):X\}$. In order to increase the crystallization degree and remove the residual NO_3^- groups, the powders obtained were annealed at 500 °C for 1 h, and a small amount of carbon powders was added into the annealment to form a reducing atmosphere. Following the same procedure above, three sets of samples with different particle sizes and doping concentrations of Tb^{3+} were prepared. The first set included four samples with the same doping concentration $[X=0.01]$ and different average sizes of 5, 10, 20, and 28 nm. The average particle size of the second set was controlled to be 10 nm and the doping concentrations of Tb^{3+} were $X=0.0005$, 0.001, 0.002, 0.005, 0.01, 0.02, 0.05, and 0.1, respectively. The average particle size of the third set was controlled to be 28 nm and the doping concentrations of Tb^{3+} were the same as the second set. Y_2O_3:Tb powder samples with a large size (>50 nm) were obtained by calcining the nanocrystal powders with sizes of 10 nm in a carbon-deoxidized atmosphere at 1000 °C for 6 h.

XRD patterns were measured with a RigakuD/max-II B x-ray diffractometer operating at 40 kV and 100 mA. Cu $K\alpha$ radiation ($\lambda=1.54$ Å) was used as an x-ray source. TEM images were obtained by using a Hitachi H-8100 transmission electron microscope. The fluorescent spectra were measured by using a Hitachi F-4500 fluorescent spectrophotometer equipped with a 150 W xenon lamp as an excitation source. In the measurement of the fluorescence decay, the fourfold frequency output of a pulsed YAG:Nd laser, 266 nm, with linewidth of 1 cm^{-1}, repetition frequency of 10 Hz, and pulse duration of 10 ns was used to excite the samples. The fluorescent signals were leaded to a French TR-550 grating monochromater and detected by a 928-type photomultiplier connected to a digital oscillograph for recording data.

III. RESULTS AND DISCUSSION

A. Structural and morphological characterization

The XRD patterns for the samples prepared by introducing different molar ratios of NO_3^- to glycine are shown in Fig. 1. Obviously, all the diffraction peaks could be assigned to those of a cubic phase of Y_2O_3 (see the JCPDS Card No. 88–1040). It can also be seen that the intensity and linewidth depend on the molar ratio of NO_3^- to glycine. The broadening of the diffraction peaks is mainly due to the decrease in the particle size. In this case, the average crystallographic sizes could be confirmed approximately by means of the Scherrer formula,[15]

$$D = k\lambda/[(\beta^2 - \beta_0^2)^{1/2}\cos\ \theta], \quad (1)$$

where k is 0.9, λ (1.54 Å) is the radiation wavelength of the copper target, β represents the full width at half maximum (FWHM) of the diffraction peak, β_0 is a modification factor for the system broadening, and θ stands for half of the diffraction position 2θ. In this calculation, the diffraction peaks at $2\theta=29.1°$ were considered and the size calculated are labeled to the corresponding curve in Fig. 1.

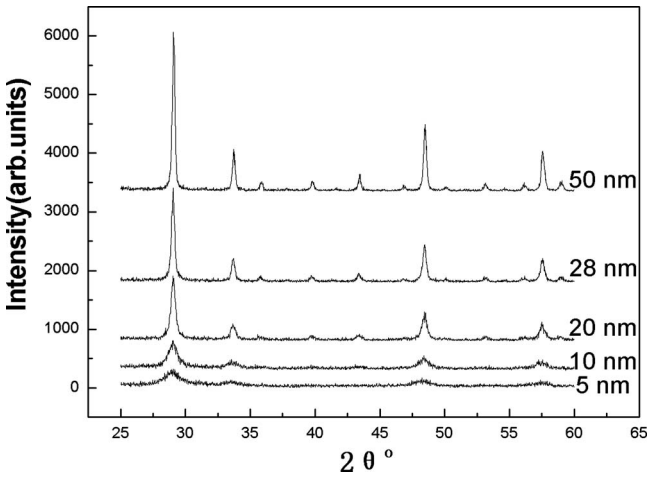

FIG. 1. XRD spectra of samples with different size ($X=0.01$).

Figure 2 shows the TEM images for the samples mentioned in Fig. 1. It is seen that the particle sizes exhibited by TEM are in good agreement with the calculation results derived from XRD. The particles have quasispherical appearance and display a narrow size distribution.

B. Dependence of excitation spectra on the particle size

The excitation spectra for the samples with the same Tb^{3+} concentration ($X=0.01$) and different particle sizes while monitoring $^5D_4 \rightarrow {}^7F_5$ emission are shown in Fig. 3(a). It shows that the excitation spectra change greatly as the particle size increases. By inspecting the excitation spectra carefully, it is found that there are four peaks located at wavelengths of around 210, 235, 273, and 303 nm for each sample of different size. The 210 nm peak in the excitation spectra can easily be assigned to the host absorption, similar

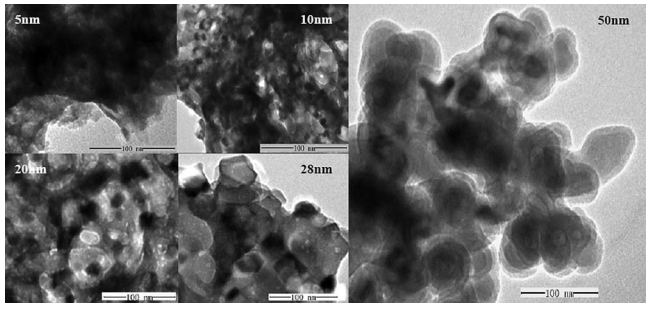

FIG. 2. TEM images for the samples with different particle size ($X=0.01$).

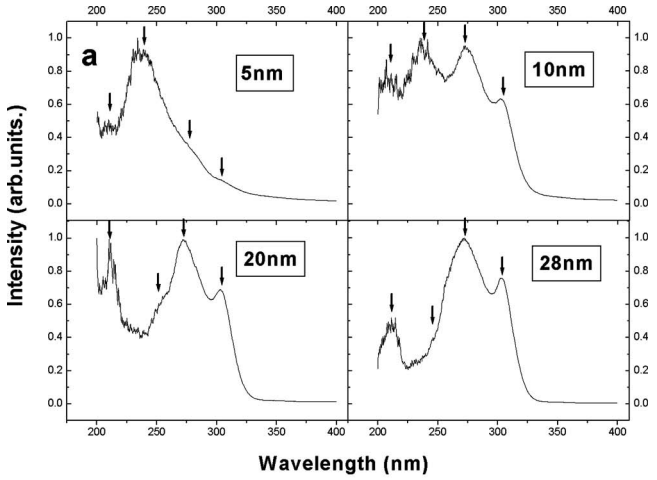

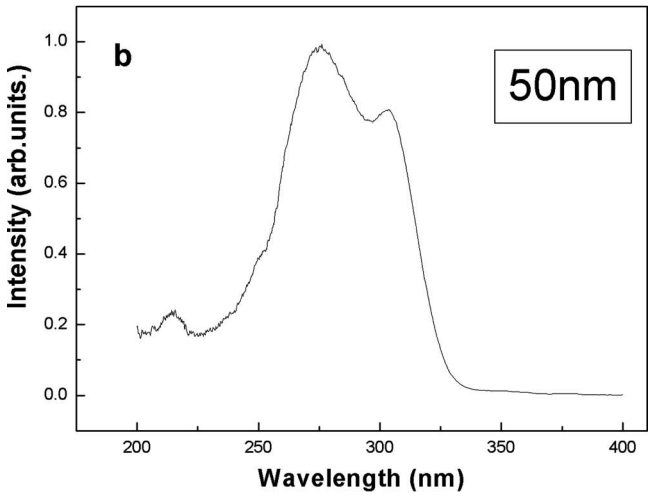

FIG. 3. Excitation spectra of the samples with different sizes, monitoring the 543 nm green fluorescent emission of $^5D_4 \rightarrow {}^7F_5$ transition of Tb^{3+} (doping concentration $X=0.01$).

to those in some other materials.[12,16] At first glance, the excitation bands in the region of ~220–250 nm are not so easy to ascribe to a reasonable origin. By comparing the excitation spectra of different-sized samples, it is found that with the decrease of the particle size the absorption band at 235 nm is intensified, and the absorption intensities for the bands at 273 and 303 nm decrease. In the case of 5 nm sample, the bands at 273 and 303 nm are degenerated as two shoulders and the 235 nm band is more intense in the spectra. Nevertheless, for the samples of a larger size (for instance, 20 or 28 nm) the excitation spectra are similar to the 50 nm sample as shown in Fig. 3(b). We know that the sample with smaller particle size has a larger ratio of surface area to volume; therefore, Tb^{3+} ions will occupy on or near surface sites with larger probability if uniform doping is taken into account. As well known, the $4f$-$5d$ transitions are different from the intra-$4f$ transitions since the $4f$-electrons are shielded by the $5s$ and $5p$ electrons. The $4f$-$5d$ transitions are more sensitive to the local environment surrounding the Tb^{3+} than the f-f transitions. The crystal field at/near the surface of nanoparticles is different from those inside the nanoparticles thanks to the disordered atomic arrangement. So, Tb^{3+} occupying these sites should display different spectra from those of the Tb^{3+} inside the particles for the $4f$-$5d$ transitions. From the experimental results and the analysis above, the excitation bands in the region of ~220–250 nm can be assigned to the intrinsic $4f^8 \rightarrow 4f^7 5d^1$ absorption of Tb^{3+} ions. Compared with the results of excitation spectra for $Y_2O_3:Tb^{3+}$ phosphors in Ref. 17, the 273 and 303 nm band can be assigned to the $4f$-$5d$ transitions of Tb^{3+} inside the nanoparticles. The 235 nm band is a new band appearing in the nanosized powders and relates to the particle size. This fact implies that the 235 nm band may be responsible for the $4f$-$5d$ transition of the Tb^{3+} at and near the surfaces.

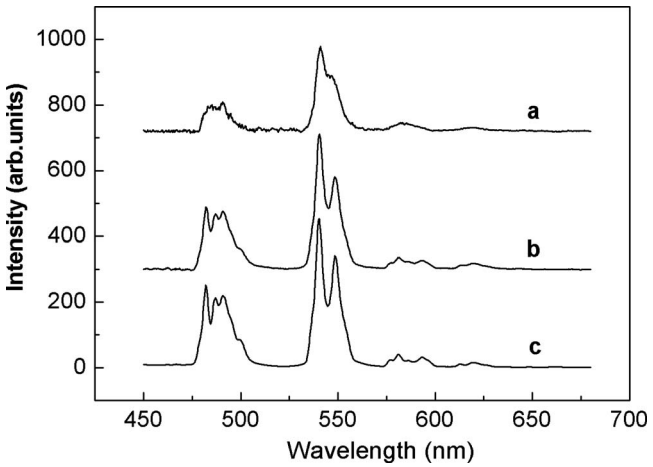

FIG. 4. Emission spectra of 10 nm sample under 235 nm (a) and 273 nm (b) excitation, and the emission spectra of 50 nm sample under 273 nm excitation (c).

In order to further validate the conclusion above, the emission spectra for the 10 nm sample were measured upon various wavelength excitations and shown in Fig. 4 as *a* and *b*. The excitation wavelengths are 235 and 273 nm, which were assigned to the absorption of $4f$-$5d$ levels of Tb^{3+} at/near the surface of nanoparticles and inside the nanoparticles, respectively. In these measurements, the same spectral resolution was kept. Figure 4 shows clearer splits of the spectral line in the emission spectrum upon 273 nm excitation, and the emission spectrum is very similar to that observed in the sample with a large size (50 nm) under 273 nm excitation [see Fig. 4(c)]. This fact means that the 273 nm excitation is mainly effective to the Tb^{3+} ions inside the nanoparticle. Under 235 nm excitation, the emission spectrum is different in that no obvious splits are observed. This emission spectrum is like the emission of Tb^{3+} in an amorphous environment. This fact tells us that the 235 nm light mainly excites the Tb^{3+} ions located at/near the particle surface, since these Tb^{3+} ions feel a crystal field like amorphous environments, due to the disordered arrangements of the atoms at/near the surfaces.

The analysis above indicates that the $4f$-$5d$ transitions of Tb^{3+} ions are more sensitive to its surroundings, so Tb^{3+} ions can be used as a probe for studying low dimensional structure materials. Furthermore, the sensitivity of $4f$-$5d$ transitions to the crystal field could be used in rebuilding energy bands for required purposes.

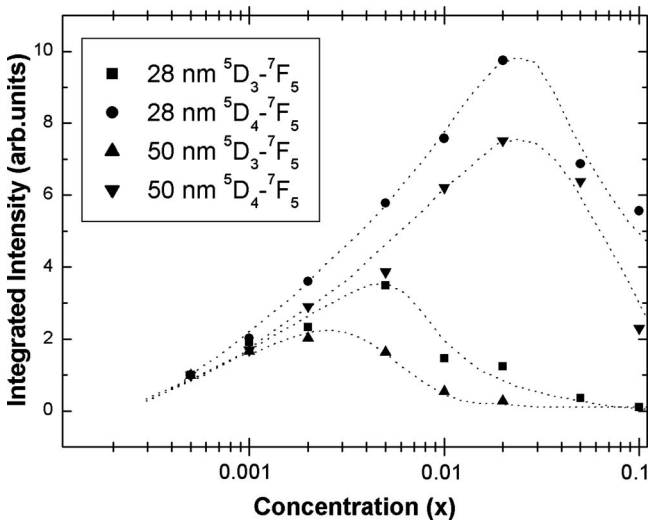

FIG. 5. The dependence of luminescent intensities for $^5D_3 \rightarrow {}^7F_5$ and $^5D_4 \rightarrow {}^7F_5$ transition on doping concentration for 28 and 50 nm samples.

C. The influence of size confinement on the energy transfer

Doping concentration is an important factor influencing the performance of the luminescent materials and should be optimized first. In this section, we intend to discover the effect of size confinement on concentration quenching and energy transfer in the nanosized $Y_2O_3:Tb^{3+}$. As stated above, the emission spectrum of 5 nm sample includes the main emission component from the Tb^{3+} ions at/near the particle surfaces. This component is different from the emission of Tb^{3+} ions inside the nanoparticles. In order to avoid the influence of Tb^{3+} ions at/near the particle surface, the samples with sizes of 28 and 50 nm and various doping concentrations were studied. The emission spectra for the samples with varied sizes under 273 nm excitation were measured under the same experimental conditions. It was observed that the spectral line shape is not dependent on the doping concentration. The integrated emission intensities for the transitions $^5D_3 \rightarrow {}^7F_5$ (423 nm) and $^5D_4 \rightarrow {}^7F_5$ (543 nm) were calculated by using numerical simulation and were normalized to the integrated emission intensity of the sample doped with Tb^{3+} $[X=0.0005]$. Figure 5 shows the dependence of integrated emission intensity on the Tb^{3+}-doping concentration for the samples with sizes of 28 and 50 nm.

Figure 5 displays that the luminescent intensity of $^5D_4 \rightarrow {}^7F_5$ transition turns the maximum intensity at almost the same doping concentration ($X=0.02$) for both 28 and 50 nm samples. However, the $^5D_3 \rightarrow {}^7F_5$ emission exhibits a different luminescent quenching process. In the 28 nm samples the luminescent quenching takes place at a doping concentration, $X=0.005$, which is higher than the concentration, $X=0.002$, found in the 50 nm samples. The different concentration quenching effect is probably due to different energy transfer mechanisms.

Huang's previous theoretical study[18] has developed a theoretical description on the relationship between the luminescent intensity and the doping concentration. Recent experimental results by Ou-Yang[19] and Li[20] have shown an agreement with the theoretical description. According to

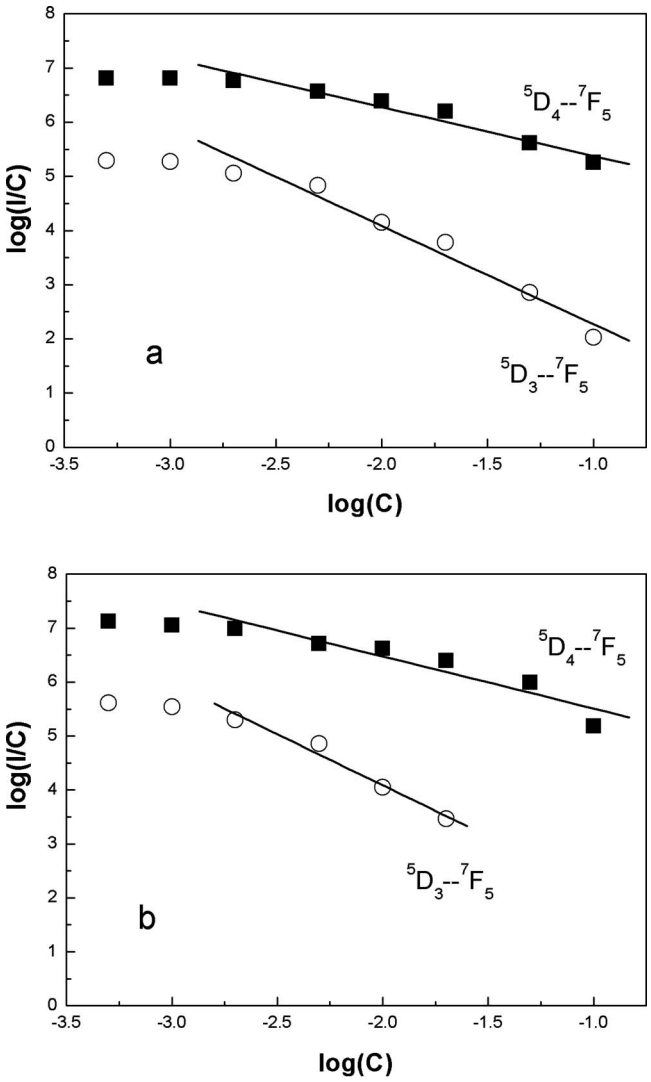

FIG. 6. $\log(I/C)$-$\log(C)$ plots for $^5D_3 \rightarrow {}^7F_5$ and $^5D_4 \rightarrow {}^7F_5$ transtion of 28 nm samples (a) and 50 nm samples (b).

Huang's results, the relationship between the luminescent intensity I and the doping concentration C can be expressed as follows:

$$I \propto a^{(1-s/d)}\Gamma(1+s/d), \tag{2}$$

$$a = C\Gamma(1-d/s)[X_0(1+A)/\gamma]^{d/s}, \tag{3}$$

where γ is the intrinsic transition probability of sensitizer, and s is the index of electric multipole, which is 6, 8, and 10 for electric dipole-dipole, electric dipole-quadrupole, and electric quadrupole-quadrupole interaction, respectively. If $s=3$, the interaction type is an exchange interaction. d is the dimension of the sample, which would equal 3 since the energy transfer between Tb^{3+} ions inside the particles is considered. A and X_0 are constants. $\Gamma(1+s/d)$ is a Γ function. From Eq. (2) and (3), it can be derived that

$$\log\left(\frac{I}{C}\right) = -\frac{s}{d}\log C + \log f, \tag{4}$$

where f is not dependent on the doping concentration.

Figure 6 shows the $\log(I/C)$-$\log(C)$ plots for the $^5D_4$

$\rightarrow {}^7F_5$ and ${}^5D_3 \rightarrow {}^7F_5$ transitions of Tb^{3+} in the 28 and 50 nm samples. According to Eq. (4), using linear fittings to deal with the experimental data in region of high concentrations, the slope parameters $-s/d$ can be obtained to be −1.81 and −1.89 for the ${}^5D_3 \rightarrow {}^7F_5$ transition in the samples with diameters of 28 and 50 nm, respectively. These slope parameters are very close to −2, so the index of the electric multipole energy transfer is 6. Therefore, the electric dipole-dipole interaction is dominant in this energy transfer. The slope parameters corresponding to the ${}^5D_4 \rightarrow {}^7F_5$ transition can be obtained to be −0.90 for the 28 nm samples, and −0.96 for the 50 nm samples, which implies that the energy transfer is of exchange interaction type. It is well known that different energy transfer types will show different distance dependencies. The effective distance of electric dipole-dipole interaction is much longer than that of exchange interaction. So, it is easy to understand the dependence of concentration quenching on the nanoparticle size. In the case of electric dipole-dipole interaction, the energy transfer can take place between the ions which are separated from each other by a longer distance (several nanometers to 10 nanometers). As the particle size decreases, the long-range energy transfer will not be existent owing to the limitation of nanoparticle boundary. Therefore, in the smaller size particles, the quenching concentration for the ${}^5D_3 \rightarrow {}^7F_5$ transition could be higher than that in the larger size particles as shown in Fig. 5. However, the decrease of particle size rarely affects concentration quenching due to the fact that the energy transfer depopulating the ${}^5D_4$ level is governed by exchange interaction, which is a short-range interaction. The effective distance of exchange interaction is only several angstroms. The nanoparticle size is approximately a hundredfold of the effective exchange interaction range. So, the influence of size confinement on exchange interaction is rather small.

D. Size- and concentration-dependence of average fluorescent lifetime

In order to verify the conclusions above, further study on the luminescent dynamic was completed. The luminescent decays for ${}^5D_3 \rightarrow {}^7F_5$ (423 nm) and ${}^5D_4 \rightarrow {}^7F_5$ (543 nm) transitions were measured under 266 nm excitation for the 28 and 50 nm samples with different concentrations ($X=0.001$ and $X=0.01$). The average fluorescent lifetime τ is defined as follows:

$$\tau = \frac{\int_{T_1}^{\infty} I(t)tdt}{\int_{T_1}^{\infty} I(t)dt}. \quad (5)$$

In Eq. (5) T_1 is the stop time of excitation, and $I(t)$ is the luminescent intensity at time t. Table I shows the average fluorescent lifetimes for different samples. It is seen that the average fluorescent lifetimes of 423 and 543 nm emissions for 28 nm samples are shorter than that of 50 nm samples at the same doping level. This result indicates that the luminescent quenching by surface defects still exists in the nanosamples. The average fluorescent lifetimes of 423 nm emission for 50 nm samples are greatly shortened as the doping concentration increases. This indicates that, as the doping concentration increases, the energy transfer probability of ${}^5D_3$ level increases. In 28 nm samples, the average fluorescent lifetime of ${}^5D_3$ level almost does not change with the increase of concentration. In the case of a lower doping level ($x=0.001$), the average fluorescent lifetime of ${}^5D_4$ level for 50 nm sample increases by about 10% compared to the 28 nm sample. In the case of a higher doping level ($x=0.01$), the average fluorescent lifetime of ${}^5D_4$ level increases by the same value. These results indicate that size confinement greatly affects the energy transfer quenching the emission from the ${}^5D_3$ level, but slightly affects the energy transfer quenching the emission from the ${}^5D_4$ level.

TABLE I. Average fluorescent lifetimes for the different size samples with different doping concentration.

Sample	*A*	*B*	*C*	*D*
Particle size (nm)	28	28	>50	>50
Tb^{3+} concentration (X)	0.001	0.01	0.001	0.01
τ 423 nm(s)	1.52×10^{-5}	1.61×10^{-5}	2.14×10^{-5}	1.73×10^{-5}
τ 543 nm(s)	1.99×10^{-3}	1.94×10^{-3}	2.19×10^{-3}	2.15×10^{-3}

IV. CONCLUSION

To conclude, we have observed that the excitation spectra corresponding to the $4f$-$5d$ transition of Tb^{3+} in nanocrystals Y_2O_3 change with the particle size. We have also found that the excitation spectra are composed of two parts: one originates from the Tb^{3+} located at/near the particle surfaces; another originates from the Tb^{3+} inside the nanoparticles. For the samples of smaller sizes, the excitation spectra are mainly dependent on the Tb^{3+} located at/near particle surface, but for the samples of larger sizes, the excitation spectra are mainly dependent on the Tb^{3+} located inside the particles. The study on concentration quenching and luminescent decay has indicated that the energy transfers depopulating the ${}^5D_3$ and ${}^5D_4$ levels were assigned to the mechanisms of electric dipole-dipole and exchange interaction, respectively. The size confinement greatly affects the energy transfer quenching the emission from the ${}^5D_3$ level, but slightly affects the energy transfer quenching the emission from the ${}^5D_4$ level.

ACKNOWLEDGMENTS

This study was partially supported by the National Natural Science Foundation of China (Grant Nos. 50572102 and 10274083), and Natural Science Foundation of Jilin Province (1999514, 20030514-2) and Outstanding Young People Foundation of Jilin Province (20040113).

[1] Y. Kojima, K. Aoyagi, and T. Yasue, J. Lumin. **115**, 13 (2005).
[2] T. Hirai and Y. Kawamura, J. Phys. Chem. B **108**, 12763 (2004).
[3] D. Chen, Y. Wang, Y. Yu, E. Ma, F. Bao, Z. Hu, and Y. Cheng, Mater. Chem. Phys. **95**, 264 (2006).
[4] Y. Zhang, Y. Li, and Y. Yin, J. Alloys Compd. **400**, 222 (2005).
[5] H. Peng, H. Song, B. Chen, S. Lu, and S. Huang, Chem. Phys. Lett. **370**, 485 (2003).
[6] H. Song, J. Wang, B. Chen, H. Peng, and S. Lu, Chem. Phys. Lett. **376**, 1 (2003).
[7] X. Mateos, R. Sole, Jna. Gavalda, M. Aguilo, J. Massons, and F. Diaz, Opt. Mater. **28**, 423 (2006).
[8] R. Hasegawa and J. Optoelectron, Adv. Mater. **6**, 503 (2004).

[9]M. Schmidt, M. Zacharias, S. Richter, P. Fischer, P. Veit, J. Blasing, and B. Breeger, Thin Solid Films **397**, 211 (2001).
[10]K. Riwotzki and M. Haase, J. Phys. Chem. B **105**, 12709 (2001).
[11]C. Yan, L. Sun, C. Liao, Y. Zhang, Y. Lu, S. Huang, and S. Lu, Appl. Phys. Lett. **82**, 3511 (2003).
[12]H. Song, B. Chen, S. Peng, and J. Zhang, Appl. Phys. Lett. **81**, 1776 (2002).
[13]Y. Tao, G. Zhao, W. Zhang, and S. Xia, Mater. Res. Bull. **32**, 501 (1997).
[14]W. Zhang, M. Xu, W. Zhang, M. Yin, Z. Qi, S. Xia, and C. Garapon, Chem. Phys. Lett. **376**, 318 (2003).
[15]J. Trojan-Piegza and E. Zych, J. Alloys Compd. **380**, 118 (2004).
[16]J. Wang, H. Song, B. Sun, X. Ren, B. Chen, and W. Xu, Chem. Phys. Lett. **379**, 507 (2003).
[17]E. Zych, J. T. Piegza, D. Hreniak, and W. Strek, J. Appl. Phys. **94**, 1318 (2003).
[18]S. Huang and L. Lou, Chin. J. Lumin. **11**, 36 (1990).
[19]F. Ou-Yang, and B. Tang, Rare Metal Mater. Eng. **32**, 522 (2003).
[20]D. Li, S. Lu, H. Wang, B. Chen, S. E, J. Zhang, and S. Huang, Chin. J. Lumin. **22**, 227 (2001).